Melekhova, L., Schlaphorst, D., Blundy, J., Kendall, J. M., Connolly, C., McCarthy, A., & Arculus, R. (2019). Lateral Variation in Crustal Structure along the Lesser Antilles Arc from Petrology of Crustal Xenoliths and Seismic Receiver Functions. *Earth and Planetary Science Letters*, *516*, 12-24. https://doi.org/10.1016/j.epsl.2019.03.030

Lateral Variation in Crustal Structure along the Lesser Antilles Arc from Petrology of Crustal Xenoliths and Seismic Receiver Functions

Elena Melekhova[1, *], David Schlaphorst[1], Jon Blundy[1], J-Michael Kendall[1], Clare Connolly[2], Anders McCarthy[1], Richard Arculus[2]

[1]School of Earth Sciences, University of Bristol, Wills Memorial Building, Bristol BS8 1RJ, UK.

[2]RSES, Australian National University, Canberra, ACT 2601, Australia

** Corresponding author, email address: lena.melekhova@bristol.ac.uk*

Abstract

We reconstruct crustal structure along the Lesser Antilles island arc using an inversion approach combining constraints from petrology of magmatic crustal xenoliths and seismic receiver functions. Xenoliths show considerable island-to-island variation in xenolith petrology from plagioclase-free ultramafic lithologies to gabbros and gabbronorites with variable proportions of amphibole, indicative of changing magma differentiation depths. Xenoliths represent predominantly cumulate compositions with equilibration depths in the range 5 to 40 km. We use xenolith mineral modes and compositions to calculate seismic velocities (v_P, v_S) and density at the estimated equilibration depths. We create a five-layer model of crustal structure for testing against receiver functions (RF) from island seismic stations along the arc. Lowermost layer (5) comprises peridotite with physical characteristics

of mantle xenoliths from Grenada. Uppermost layer (1) consists of 5 km of volcaniclastics and sediments, whose physical properties are determined via a grid inversion routine. The three middle layers (2) to (4) comprise igneous arc crust with compositions corresponding to the xenoliths sampled at each island. By inversion we obtain a petrological best-fit for the RF on each island to establish the nature and thicknesses of layers (2) to (4).

Along the arc we see variations in the depth and strength of both Moho and mid-crustal discontinuity (MCD) on length-scales of tens of km. Moho depths vary from 25 to 37 km; MCD from 11 and 32 km. The Moho is the dominant discontinuity beneath some islands (St. Kitts, Guadeloupe, Martinique, Grenada), whereas the MCD dominates beneath others (Saba, St. Eustatius). Along-arc variability in MCD depth and strength is consistent with variation in estimated magmatic H_2O contents and differentiations depths that, in turn, influence xenolith lithologies. A striking feature is steep, along-arc gradients in v_P similar to those observed at other oceanic arcs. These gradients reflect abrupt changes in rates and processes of magma generation in the underlying crust and mantle. We find no evidence for large, interconnected bodies of partial melt beneath the Lesser Antilles. Instead, the crustal velocity structure is consistent with magma differentiation in vertically-extensive, crystal mush-dominated reservoirs. Along-arc variation in crustal structure may reflect heterogeneous upwelling within the mantle wedge, itself driven by variation in slab-derived H_2O fluxes.

Highlights

- Arc crustal structure modelled by integrating petrology of 230 igneous xenoliths with seismic data from 23 islands
- Crust comprises four layers defined on basis of xenolith composition, calculated seismic properties and receiver functions

- Steep lateral velocity gradients and irregular along-arc variations in depth to Moho and mid-crustal discontinuity
- Lateral variation consistent with island-to-island variation in xenolith petrology
- Velocity structure reflects heterogeneous upwelling within the mantle wedge, driven by variation in slab-derived H_2O fluxes

Keywords: *island arc; crustal structure; magma differentiation; xenoliths; seismic properties of rocks; receiver functions*

1. Introduction

1.1 Background

The layered nature of Earth's continental crust is the time-integrated product of magmatic differentiation (Rudnick & Fountain, 1995). At convergent margin sites of active crust formation, subducted slabs release H_2O-rich fluids into the mantle wedge, inducing partial melting of peridotite to generates hydrous magmas of broadly basaltic composition. Subsequent magmatic differentiation converts mantle-derived basalts into more evolved compositions (e.g., andesites, granites) characteristic of mature continental crust. In the early stages of differentiation Mg-rich mineral phases (olivine, pyroxenes) separate as ultramafic cumulates from increasingly silica-rich melts. The appearance of plagioclase is delayed due to the hydrous nature of the parent basalt, such that gabbroic (plagioclase-bearing) cumulates only appear after ~40% crystallisation and andesitic melts with ~60 wt% SiO_2 after ~70% crystallisation (Nandedkar et al., 2014). The exact proportions depend on the original magmatic H_2O contents, differentiation depths and styles, and the extent of assimilation of older crust. Regardless of these details, chemical differentiation at arcs generates significant

volumes of mafic and ultramafic solid residues. For bulk crustal compositions to become broadly andesitic (Rudnick & Fountain, 1995) requires that some residual material is displaced into the underlying mantle, either by downwards foundering ('delamination' – Jull & Kelemen, 2001) or by upwards migration of the seismic Moho to coincide with the appearance of plagioclase.

The constitution of the crust can be elucidated through studies of exhumed arc sections (e.g., Jagoutz & Behn, 2013), crustal xenoliths in volcanic rocks, or geophysical properties (e.g., Shillington et al., 2004; Kodaira et al., 2007). There is consensus that the continental crust comprises at least three layers, characterised by downwards increasing P-wave velocities (Rudnick & Fountain, 1995). Middle crust has an andesitic composition (61 wt% SiO_2; 3 wt% MgO), whereas lower crust is more mafic (52% SiO_2; 7% MgO). The uppermost crust is predominantly felsic igneous (66% SiO_2, 2% MgO), although the prevalence of variously fractured and unconsolidated volcanic and sedimentary rocks complicates the picture. For this reason, it is reasonable to divide the upper layer into an igneous lower part and a volcanic-sedimentary upper part. Some part of arc crust may comprise pre-existing, overriding plate upon which the magmatic arc was built, although recent studies in western Mognolia and the Izu Bonin Mariana arc (Gianola et al., 2017; Ishizuka et al., 2018) suggest such material is conspicuously absent.

Globally, crustal thickness and velocity structure of oceanic arcs is highly variable (Fig. 1). Some arcs conform to a simple three-layer structure (e.g., Sunda, Kermadec, New Britain), whereas others are more complex (e.g., Mariana, Aleutians, New Ireland). The Moho is not always well-resolved (e.g., Lesser and Greater Antilles). The apparent diversity of arc

98 structure, both between and within oceanic arcs, suggests significant complexity in crust
99 formation and evolution.
100
101 Resolving crustal structure is both a geophysical and petrological problem. Whereas
102 geophysics can resolve vertical and lateral variation in rock properties (v_P, v_S, density), their
103 interpretation in terms of igneous processes and lithologies requires a petrological
104 framework. To provide such a framework, we take as our study site the Lesser Antilles arc
105 (LAA), an active, slow-subduction intra-oceanic arc that is well instrumented geophysically,
106 well characterised geologically, and known to show significant along arc variation in
107 structure and petrology (Fig. 1, Boynton et al., 1979; Arculus & Wills, 1980). We combine
108 petrology and mineralogy of more than 200 crustal xenoliths from eleven volcanic islands
109 along LAA with seismic data from 23 remote island stations to investigate crustal structure in
110 such a way that one approach informs the other. We compare our findings to other oceanic
111 arcs and speculate on crustal structure and crust-forming processes more generally.
112

113 ### *1.2 The Lesser Antilles*

114 The LAA is an active, mature, intra-oceanic arc extending ~750 km from South America to
115 the Greater Antilles. The arc is a manifestation of slow, westward subduction of the North
116 and South American plates beneath the Caribbean plate. A review of the geological,
117 geochemical and tectonic setting of LAA is provided by Macdonald et al. (2002) and Smith
118 et al. (2013). LAA crustal structure was summarised by Schlaphorst et al. (2018).
119
120 LAA comprises eleven major volcanic islands and an archipelago of nineteen small islands
121 (the Grenadines) between St. Vincent and Grenada (Fig. 2). The arc bifurcates north of
122 Martinique producing inactive eastern and active western limbs. The active arc can be

123 divided into northern, central and southern segments with Wadati-Benioff zone dips varying
124 from 50-60° in the north to sub-vertical in the south. Over the last 0.1 Ma volcanism has been
125 more prominent in the central segment, as reflected in larger volcanic edifices. Average
126 magma production rates (162 $km^3km^{-1}Myr^{-1}$; Jicha & Jagoutz, 2015) fall at the lower end of
127 intra-oceanic arcs worldwide.
128
129 Compositions of LAA volcanic and plutonic rocks span the global arc array (Fig. 3), from
130 MgO-rich picrites and ankaramites on some islands (e.g., St. Vincent, Grenada, Martinique)
131 to voluminous dacites and rhyodacites on others (e.g., Dominica, St. Lucia). The northern and
132 central segments are predominantly andesitic with minor basalt, dacite and rare rhyolite (e.g.,
133 Toothill et al., 2006). The southern segment is dominated by basalts and basaltic-andesites,
134 including primitive, hydrous, MgO-rich (>12 wt%) basalts (e.g., Macdonald et al. 2002). The
135 high (>20 wt%) Al_2O_3 contents of basalts (Fig. 3b) reflect elevated magmatic H_2O contents.
136 On the basis of Fe-Mg partitioning between olivine and melt for magmas of known
137 Fe_2O_3/FeO, truly primitive magmas, i.e. those in equilibrium with olivine $Fo_{\geq 90}$, are limited
138 almost entirely to basalts (≤50 wt SiO_2) from the southern segment (Fig. 3c). Very few more
139 evolved magmas, e.g. basaltic andesites (≤55 wt SiO_2), may also be primitive. Isotopic data
140 show that the magmatic history of most LAA islands is dominated by igneous differentiation
141 processes with limited assimilation of older sialic crust or sediments (e.g., Macdonald et al.
142 2002; Toothill et al., 2006; Tollan et al., 2012; Bezard et al., 2014). Crustal contamination is
143 most pronounced on St. Lucia and Martinique (Bezard et al., 2015).
144
145 Igneous xenoliths occur on all LAA islands (Wills, 1974; Arculus & Wills, 1980). Xenoliths
146 are mineralogically and texturally diverse, both within individual islands and along the arc
147 (e.g., Arculus & Wills, 1980; Cooper et al., 2016; Camejo-Harry et al., 2018). Melekhova et

al. (2017) subdivide xenoliths into those that represent instantaneous solid extracts from one or more magma batches ("cumulates") and those whose compositions match erupted lavas and have mineralogies and textures consistent with protracted solidification of magma ("plutonics"). Cumulate xenoliths may contain significant quantities of trapped melt (e.g. Stamper et al., 2014) and it is likely that there is a continuum from cumulate to plutonic types according to this simple terminology. Geobarometry of LAA cumulate xenoliths (e.g., Stamper et al., 2014; Ziberna et al., 2017; Melekhova et al., 2017) yields crystallisation pressures between 2 and 10 kbar, indicating that xenoliths sample igneous crust over a significant depth range.

The LAA has been the subject of several major geophysical experiments (Boynton et al., 1979; Christeson et al., 2008; Kopp et al., 2011; Laigle et al., 2013), summarised in Figure 1, and a recent study of along-arc variations in crustal thickness using receiver functions (Arnaiz-Rodrígues et al., 2016). Estimated crustal thickness ranges from 22 to 37 km. Boynton et al. (1979) identified two seismic refractors that subdivide the crust into layers. Their upper crustal layer is of plutonic igneous origin (Wadge, 1986) with an average v_P of 6.2 $km \cdot s^{-1}$; its base varies significantly in depth (2 to 20 km) along strike. The uppermost portion of the upper layer has lower seismic velocities (v_P <6 $km \cdot s^{-1}$) and densities and is likely composed of volcaniclastic and sedimentary rocks with abundant fractures and pores (Kiddle et al., 2010; Kopp et al., 2011). Gravity data from Guadeloupe (Gailler et al., 2013) show that this layer is approximately 4 km thick. The lower crustal layer of Boynton et al. (1979), immediately overlying the mantle, has average v_P = 6.9 $km \cdot s^{-1}$ and is thought to represent dense mafic igneous rocks, including cumulates.

Kopp et al. (2011) and Christeson et al. (2008) produced detailed seismic models of crustal structure between Dominica and Guadeloupe and south of Grenada respectively. They confirmed a layered crustal structure to that proposed by Boynton et al. (1979), albeit with smoother vertical velocity gradient. For both profiles sub-arc v_P ranges from 1.4 to 7.3 km/s, with most crust having v_P of 5.2 to 7.3 km/s (Fig. 1). Neither survey was able to constrain well the sub-arc Moho.

2. Crustal xenoliths

During five field campaigns (2009-2017) we sampled every island in LAA, recovering just under 900 coarse-grained igneous xenoliths both in situ and, predominantly, ex situ in river drainages and reworked volcanic deposits. Xenoliths display great variation in mineralogy and texture (Fig. 4) from hornblendite and wehrlite through gabbro and troctolite to quartz-hornblende leuconorite and diorite (e.g., Wills, 1974; Arculus & Wills, 1980, Kiddle et al., 2010, Stamper et al., 2014). The ubiquity of igneous xenoliths suggest that they represent building blocks of LAA crust, providing a window into the entire differentiation history of arc magmas from their source to eruption. Diversity in xenolith mineralogy reflects variation in the composition of mantle-derived parent magmas, especially H_2O contents, and the differentiation paths they follow through the crust (Melekhova et al., 2015).

2.1 Xenolith assemblages and modes

Despite their textural diversity, the mineralogy of crustal xenoliths is relatively straightforward. More than 99% comprise permutations of eight mineral groups: olivine, clinopyroxene, orthopyroxene, amphibole, plagioclase, magnetite, ilmenite and quartz. Relative modal abundances of plagioclase and amphibole are significant (Fig. 5) and

196 plagioclase-free assemblages are uncommon, found only on Grenada, Bequia and St.
197 Vincent. Accessory minerals include apatite, analcime, biotite, sulphides and zircon.
198
199 Graphical comparison of xenolith mineral modes of from eleven islands is shown in Figure 5.
200 The overall mafic (plagioclase-poor) character of xenoliths from the southern islands of
201 Grenada, Carriacou and Bequia stands in sharp contrast to the predominance of felsic phases
202 (notably plagioclase) in St. Kitts, Montserrat, Guadeloupe and St. Lucia. Orthopyroxene is
203 rare or absent from southern islands xenoliths. The main mineral assemblages and textures,
204 from south to north, are as follows (cf. Arculus & Wills, 1980).
205 *Grenada* xenoliths are dominated by mafic minerals with abundant hornblende and
206 clinopyroxene and include plagioclase-free varieties (Fig. 4a) that are otherwise rare
207 (Stamper et al., 2014). Orthopyroxene is lacking; iddingsitised olivine is common. Most
208 xenoliths have adcumulate textures.
209 *Carriacou* xenoliths are dominated by clinopyroxene, amphibole and plagioclase. Olivine is
210 uncommon; orthopyroxene is lacking. A distinct feature is the presence of quartz and apatite
211 in diorites, the abundance of sulphides, and presence of interstitial analcime in few samples.
212 Textures range from adcumulates to porphyritic-phaneritic (Fig. 4b) and granoblastic
213 varieties.
214 *Bequia* xenoliths have the most diverse assemblages from a single island ranging from
215 ultramafic to felsic (≤75wt% plagioclase), with olivine (iddingsitized), amphibole,
216 clinopyroxene, plagioclase and spinel plus rare orthopyroxene and ilmenite. Textures range
217 from adcumulate to orthocumulate with variable crystallisation sequences (Camejo-Harry et
218 al., 2018).
219 *St. Vincent* xenoliths are characterised by abundant olivine and negligible orthopyroxene with
220 well-equilibrated, predominantly adcumulate textures and a lack of mineral zoning (Tollan et

al., 2012). Distinctive features include the presence of troctolites, with or without hornblende (Fig. 4c), and olivine hornblendites.

St. Lucia xenoliths differ from other southern islands in being very evolved (high Fe/Mg) and dominated by amphibole and plagioclase. Olivine is rare, orthopyroxene predominates over clinopyroxene (Fig. 4d), and quartz and biotite are common. Cumulate textures are rare; most samples resemble quenched mushes with abundant interstitial material.

Martinique xenoliths are predominantly igneous, with sparse cordierite-bearing hornfelses. All xenoliths are plagioclase-bearing, with variable proportions of olivine (troctolites), clinopyroxene, orthopyroxene, amphibole and spinel, commonly with interstitial melt (Cooper et al., 2016).

Dominica xenoliths show low variability assemblages dominated by olivine, clinopyroxene and plagioclase (Fig. 4e), often with well-equilibrated textures (Ziberna et al., 2017) that resemble those on Carriacou. Olivine is partially iddingsitized.

Guadeloupe xenoliths are dominated modally by plagioclase. Relatively primitive samples contain varying proportions of olivine, pyroxene, amphibole, and spinel, whereas more evolved samples contain quartz, biotite, magnetite, ilmenite, apatite, orthoclase, sulfide and rare zircon (Fig. 4f). Most xenoliths appear isotropic and homogeneous, yet texturally diverse, with both igneous and metamorphic (hornfelsed) varieties.

Montserrat xenoliths, similar to Guadeloupe and St. Lucia, are distinctively felsic and olivine-free. Assemblages are dominated by noritic and gabbroic anorthosites and hornblende-gabbros. Other common varieties include quartz-diorite and metamorphosed biotite-gabbro. Cumulate and crescumulate textures abound (Kiddle et al., 2010).

St. Kitts xenoliths are dominated by exceptionally calcic plagioclase ($An_{\leq 100}$; Melekhova et al., 2017) and amphibole, typically in reaction relationship with pyroxene and olivine. Both cumulate and plutonic varieties occur. Important characteristics include the presence of two

pyroxenes, biotite, apatite, and coexisting ilmenite and magnetite. Interstitial melt is common.

St. Eustatius mineral assemblages and textures are similar to those of Martinique (Cooper et al., submitted). Orthopyroxene occurs only in non-cumulate (plutonic) gabbros.

3. Methods

3.1 Petrological constraints: physical properties of crustal xenoliths

Fifty to seventy xenoliths per island were studied and divided into textural and mineralogical groups from which representative samples were analysed. Mineral major element chemistry was analysed on polished carbon-coated thin-sections using Cameca SX100 and JEOL 8530F electron microprobes at University of Bristol and the Australian National University respectively. Analytical conditions were 15 or 20 kV accelerating voltage and 10 nA focused beam. Modal abundances of major mineral phases (≥0.5 vol%) were obtained by point-counting (900 to 3000 points per thin-section). Volume modes were converted into mass fraction modes using appropriate mineral densities.

Physical properties of rocks (v_P, v_S, density) can be calculated from mineral compositions and proportions, provided that a reasonable estimate of temperature and pressure are available (e.g., Müntener and Ulmer, 2006, Jagoutz and Behn, 2013). We retrieved physical properties of LAA xenoliths, using their mass fraction modes and mineral compositions, with the algorithm of Hacker & Abers (2016) for the nine major islands with seismic stations: Grenada (Stamper et al., 2014); St. Vincent (Tollan et al., 2012); St. Lucia (Wills, 1974 and our unpublished data); Martinique (Cooper et al., 2016); Dominica (Wills, 1974); Guadeloupe (our unpublished data); Montserrat (Kiddle et al., 2010); St. Kitts (Melekhova et al., 2017); and St. Eustatius (Cooper et al., submitted). Modal abundances for each island are

271 reported in Supplementary Table S2. For all solid solutions we calculated the proportions of
272 end-members; for amphibole we used the generic "hornblende" in the Hacker & Abers
273 (2016) database. The modal proportion of quartz is consistently very low, making distinction
274 between **α**-quartz and **β**-quartz (cf. Jagoutz & Behn, 2013) immaterial for calculating
275 physical properties
276
277 Pressure-temperature (P–T) conditions of xenolith equilibration were estimated using a
278 variety of geobarometers and geothermometers (e.g., Ziberna et al., 2017; Supplementary
279 Tab. S2), together with constraints from phase equilibrium experiments performed on
280 appropriate starting compositions (cf. Stamper et al., 2014). For the majority of islands
281 studied magmatic H_2O contents were estimated based on melt inclusion analyses (Bouvier et
282 al., 2008, Melekhova et al, 2017, Cooper et al., submitted). Knowing H_2O content, phase
283 assemblages and mineral composition of studied xenoliths (particularly, Fo content of olivine
284 and An content of plagioclase) helped us to narrow the existing experimental dataset (~1500
285 experiments) to obtain reliable P and T. The full dataset of calculated physical properties and
286 P-T estimates, including methods used and uncertainties, is given in Supplementary Table S2.
287 Because of the counteracting effects of increasing P and T on physical properties, realistic
288 deviations from estimated P-T values have little bearing on the calculated properties, i.e. <1%
289 relative in v_P and <0.008 in v_P / v_S ratio. We also calculated physical properties of peridotite
290 beneath LAA using mantle xenoliths from Grenada (Parkinson et al., 2003; Stamper et al.,
291 2014). Mantle xenoliths are not found on any other island in the LAA.
292

293 ### *3.1 Geophysical constraints: seismic properties and structure*

294 Broadband seismic data from various regional networks were collected (Fig. 2); for
295 Montserrat, Guadeloupe and Martinique more than one station is available. Teleseismic

296 events were filtered using a 2nd order Butterworth bandpass filter from 0.4 Hz to 3 Hz and
297 only events with a clear P-phase were selected (Schlaphorst et al., 2018). We use the
298 extended-time multi-taper frequency-domain cross-correlation receiver-function (ETMTRF)
299 of Helffrich (2006) and an H–κ stacking method similar to Thompson et al. (2010). H–κ
300 stacking is based on theoretical arrival times of converted phases and derives values for the
301 depth (H) to a seismic discontinuity and the average P-wave to S-wave ratio ($\kappa=v_P/v_S$) of the
302 overlying crustal layer. As noted by Schlaphorst et al. (2018), a significant disadvantage of
303 H–κ stacking is its reliance on a single discontinuity separating two layers, such as upper and
304 lower crust (mid-crustal discontinuity - MCD) or crust and mantle (Moho). In the case of
305 layered crust with multiple discontinuities peaks in the RF caused by different discontinuities
306 can overlie each other, complicating the H–κ stacking results. For example, on Martinique,
307 H–κ stacking shows a strong, well-resolved discontinuity at 28.3 ± 1.1 km (Fig. 3a), whereas
308 on St. Lucia, the discontinuity is placed much deeper (46.5 ± 1.8 km) and the solution is very
309 poorly resolved. At some islands H values are too shallow, producing unrealistic depths to
310 the Moho or missing it altogether. Schlaphorst et al. (2018) concluded that H–κ stacking
311 results for layered crust can be easily misinterpreted and proposed an inversion modelling
312 approach to overcome this problem. In combination with petrology, their approach provides a
313 powerful tool to distinguish between one or more MCD and the Moho, and to resolve the
314 seismic properties (v_P, v_P/v_S) of multiple layers, even at island seismic stations with relatively
315 high noise.
316
317 We apply a combination of the grid-search and inversion methods of Schlaphorst et al. (2018)
318 to the RF assuming a four-layer crust plus underlying mantle within the following
319 petrological framework: uppermost crustal layer (1) composed of loosely consolidated and

fractured volcaniclastic rocks, sediments and lavas; upper (2), middle (3) and lower (4) crustal layers composed of plutonic igneous rocks; and a peridotitic mantle layer (5).

Physical properties of surface layer (1) are controlled primarily by fracture density and degree of consolidation, rather than the lithology *per se*. Therefore, for layer (1), we first invert the RF using the method of Ammon et al. (1990) assuming five 1-km thick subsidiary layers (1a-e). Total thickness of layer (1) is fixed at 5 km, consistent with the geophysical data of Christeson et al. (2008), Kiddle et al. (2010) and Gailler et al. (2013).

Crustal layers (2), (3) and (4) consist of the various xenolith lithologies for which physical properties were calculated. Beneath each island we identify a range of plausible lithologies for each of the three layers, based on our P-T estimates (Fig. 6c, Supplementary Tab. S2). On the basis of our textural observations and thermobarometric calculations layer (4) is found to be consistently cumulate in character, whereas layers (2) and (3) represent mixtures of cumulate and plutonic (solidified magmas or mushes) lithologies (Supplementary Tab. S2). We then perform a grid-search using the calculated v_P, v_S, v_P/v_S and density of each lithology to find those that yields a best-fit to the RF for that island. We assume that all melt has either been extracted or is isolated at very low melt fraction along grain boundaries, consistent with the low melt fractions observed in xenoliths (see below).

Physical properties of mantle layer (5) were based on Grenadian peridotite xenoliths (Parkinson et al., 2003; Stamper et al., 2014): v_P=8.00 km·s^{-1}, v_S=4.43 km·s^{-1}, rho=3.33 kg·m^{-3}. The same values were used for the entire LAA as there is insufficient evidence from petrology or seismology to justify along-arc variation in mantle v_P. For comparison the

seismic profiles of Christeson et al (2008) and Kopp et al. (2011) yield sub-arc mantle v_P of 7.7 km/s and 8.0 km/s, respectively.

4. Results

Our physical property calculations indicate that the permissible range of v_P/v_S for each island is narrow (Fig. 6a, Supplementary Tab. S2). On average, v_P/v_S varies between 1.79 to 1.88 for v_P from 6.2 to 7.4 $km \cdot s^{-1}$ (Fig. 6 a & b and Supplementary Tab. S2). In contrast to Müntener & Ulmer (2006) calculated xenolith v_P values never exceed 7.8 $km \cdot s^{-1}$ and are therefore consistently lower than the mantle (Fig. 6a). The relationship between density and v_P is non-linear (Fig. 6b). Densities of mantle xenoliths from Grenada and ultramafic crustal xenoliths from Grenada and St Vincent are similar, ~ 3.3 g/cm^3, however the majority of LAA crustal xenoliths has a narrow range of densities, 2.8-3.0 g/cm^3. Lithologies dominated by amphibole + plagioclase ± quartz result in v_P values down to 6.2 $km \cdot s^{-1}$, with relatively low v_P/v_S (Fig. 6a), whereas calculated v_P/v_S for plagioclase-dominated lithologies (≥80%) are up to 1.91 at comparable v_P (Fig. 6a).

Depth distribution of LAA xenoliths (Fig. 6c) suggests that v_P of the igneous crust is variable: 6.2 to 7.0 $km \cdot s^{-1}$ in layer (2), 6.4 to 7.2 $km \cdot s^{-1}$ in layer (3) and 6.8 to 7.4 $km \cdot s^{-1}$ in layer (4). The range of xenolith physical properties (v_P, v_S, v_P/v_S, density) and depth ranges define the petrological parameter space of our grid-search method to find the combination of lithology and thickness for each crustal layer beneath each island that best fits the corresponding RF. Despite our extensive sampling, on the islands of St. Lucia and St. Eustatius, we have no xenolithic record of potential lower crustal lithologies. Initial models for these two islands were therefore run without layer (4). However, a good fit to RF was not achieved, so we introduced a plausible lower crust layer (4) taking values from neighbouring

St. Vincent and St. Kitts respectively. On any island (e.g. Montserrat) where the best-fit thickness of a given layer lay within error of zero this layer was omitted, reducing to a three-layer crustal structure. Our inversion approach considers only new, magmatic arc crust. Schlaphorst et al. (2018) demonstrated that incorporating a layer of vestigial proto-Caribbean crust (pCc) into the crustal model does not change the depth of the discontinuities in the inversion results unless the pCc is unrealistically thick (≥20 km).

Representative best-fit model velocity profiles and synthetic RF for two islands (Martinique and Grenada) are illustrated in Figure 7. For Martinique two strong discontinuities at 27 km (Moho) and 13 km (MCD1) were identified (Fig.7a). A weak additional discontinuity (MCD2) lies just above the Moho at 24 km depth. The best fit for Martinique was achieved with the following lithologies: layer (2) troctolite, (3) olivine gabbro and (4) hornblende gabbronorite. For Grenada, the Moho is identified at 29 km and both MCDs are strong (12 and 14 km) with a small intervening low velocity zone (Figs.7b and 8). The best fit for Grenada was achieved with following lithologies: layer (2) poikilitic-hornblende gabbro, (3) hornblende gabbro and (4) clinopyroxene hornblendite. Modelled velocity profiles and RF for all studied islands, obtained as for Martinique and Grenada, are provided in Supplementary Material and summarised in terms of crustal lithologies in Table 1.

5. Crustal structure of the Lesser Antilles arc

The v_P, v_S, v_P/v_S and density constraints from xenolith petrology combined with RF inversion provide new insights into LAA velocity structure (Figs. 8). MCD depths and v_P for layers (2) to (4) are in an excellent agreement with previous work on the southern segment of the arc (Fig.1 and Schlaphorst et al., 2018). The Moho was not directly observed seismically in previous studies but was estimated to lie between 24 and 35 km depth (e.g., Boynton et al.

1979; Christeson et al., 2008; Kopp et al., 2011; Laigle et al., 2013; Arnaiz-Rodrígues et al., 2016).

Our obtained crustal structure (Fig. 8) shows that MCD and Moho depths are highly variable over surprisingly short, along-arc distances of tens of kilometres. Arnaiz-Rodrígues et al. (2016) arrived at a similar conclusion, with up to 10 km change in Moho depth across Guadeloupe alone. Our Moho depths vary from 24 km (St. Eustatius) to 38 km (e.g. St. Kitts and Dominica). The seismic velocity of layers (2), (3) and (4) also varies laterally. The modelled four-layer crustal structure yields two MCD, however one of them is usually stronger than the other. Depth to the MCD between layers (3) and (4) changes from 12 to 32 km, whilst that between layers (2) and (3) is from 6 to 15 km. Beneath St. Lucia, layer (2) is very thin (~2 km); beneath Montserrat it is absent. Beneath Grenada 2 km-thick layer (3) has a lower v_P than overlying layer (2); St. Eustatius has a very thin (1 km) layer (4) with lower v_P than overlying layer (3). Variation in v_P along the arc is non-systematic. For example, we observe a high v_P mid-crustal layer (3) under Martinique and St. Eustatius (6.97 and 7.14 km/s respectively), but a low layer (3) v_P of 6.55 km/s under Grenada (Figs. 8 and 9). Lower crustal layer (4) v_P varies from 7.43 km/s beneath Montserrat to 6.75 km/s beneath St. Kitts just 90 km to the north. Our along-arc variability in discontinuity depths (Fig. 8) is similar to that of Boynton et al. (1979).

Our preferred final, five-layer P-wave velocity model (Fig. 8) for LAA is as follows. The 5 km-thick upper layer (1) has highly variable v_P due to lithological heterogeneity. P-wave velocities are 6.2 to 6.86 $km \cdot s^{-1}$ in the upper crust (layer 2) in the depth range of 6 to 15 km, 6.46 to 7.18 $km \cdot s^{-1}$ in the middle crust (layer 3) in the depth range 12 to 32 km, and 6.75 to 7.43 $km \cdot s^{-1}$ in the lower crust (layer 4) in the depth range 26 to 38 km.

5. Interpretation and discussion

Our petrologically-informed crustal model for LAA (Fig. 8) resembles that of other oceanic island arcs (Fig. 1) including those, subject to high-resolution seismic experiments, such as the northern segment of Izu-Bonin (Kodaira et al. 2007) and the Aleutians (Shillington et al 2004). To facilitate comparison of LAA with these two arcs, in Figure 9 we present seismic velocity profiles for all three arcs using the same vertical and horizontal scales and consistent v_P contour intervals of <6 km·s^{-1}, 6.0-6.8 km·s^{-1}, 6.8-7.8 km·s^{-1} and >7.8 km·s^{-1}.

Several key features emerge. Like LAA, the northern segment of Izu-Bonin and the Aleutians show the expected downwards increase in v_P, together with abrupt lateral variations on wavelengths of a few tens of km, as previously noted by Kodaira et al. (2007). Both the 6.8 km s^{-1} and 7.8 km s^{-1} contours show considerable along-arc variation in depth, by up to 20 km. Beneath some volcanic islands (e.g., Dominica and Montserrat in LAA; South Sumisu and Nii-jima in Izu-Bonin; Unalaska and Chuginadak in Aleutians) material with v_P in the range 6.8-7.8 km·s^{-1} extends to very shallow crustal depths, in some cases impinging almost directly on crustal layer (1). In all three arcs there is no clear correlation between the depths to the 6.8 and 7.8 km s^{-1} contours, suggestive of strong decoupling between thicknesses of the different crustal layers. Despite the greater spatial resolution of the crustal structure in Izu-Bonin and Aleutians arcs (Fig. 9), it would appear that the crust in all three arcs displays the same abrupt lateral variations in physical properties. The diversity of crustal lithologies, as recorded by xenoliths, is responsible for the change of seismic properties along the LAA (Figs. 5, 6 and 8). Lateral variations in v_P in Izu-Bonin and Aleutians may have a similar lithological cause, although there is not the same xenolith record with which to evaluate this possibility.

Tamura et al. (2016) compared crustal thickness along the Izu-Bonin arc, obtained from seismology, with bathymetry. They found a correlation between water depth and crustal thickness, suggesting that water depth can be used to estimate crustal thickness under the arc. They ascribe this variation to changes in the nature of mantle-derived magmas, from basalt to andesite, along the arc. We constructed the along-arc profile for LAA using bathymetric data for the eastern Caribbean (Fig. 8). Although there is some correlation, it is not as uniform and straightforward as shown for Izu-Bonin by Tamura et al. (2016), perhaps reflecting the lower spatial resolution of our study. Nonetheless, water depth and crustal thickness link well for the southern segment of the arc and for Dominica and Guadeloupe, the largest islands with the greatest crustal thickness. The most obvious misfit is Martinique, where, despite the island's considerable size, the crust is relatively thin.

Geochemical data from LAA (Fig. 3c) do not support a wide variety of mantle-derived magmas along the arc, in contrast to the proposition of Tamura et al. (2016) for Izu-Bonin. The relationship between our calculated crustal structure and magmatic history (magma compositions, fluxes, volatile contents etc) of each island in LAA remains to be investigated. However, we can speculate as to possible explanations for along-arc lithological changes.

Variations in v_P could arise through variations in trapped melt fraction within rocks of broadly similar seismic velocities. The presence of partial melt reduces both v_P and v_S, but increases v_P/v_S significantly, due to the stronger reduction of v_S. The extent of v_P/v_S reduction depends not only on melt fraction, but also on its distribution. In regions with significant, distributed partial melt v_P/v_S ratios of up to 2.00 are observed (Hammond et al., 2011). However, LAA islands whose H–κ stacking results agree with those from RF inversion (e.g.

469 Montserrat, Martinique) indicate v_P/v_S significantly less than 2, suggesting rather little
470 interconnected partial melt. In their H–K stacking study of the LAA Arnaiz-Rodrigues et al.
471 (2016) also found v_P/v_S consistently in the range 1.77-1.87. Melt-rich regions of reduced v_P
472 would correspond to increased v_P/v_S in Figure 8. If melts are fully interconnected, i.e. melt
473 wets grain boundaries completely, then it is possible to calculate their effect on v_P and v_P/v_S.
474 Using the experimental data of Chantel et al. (2016) for anhydrous basaltic melt in an olivine
475 matrix, we calculate that 5 vol% of fully interconnected melt will reduce v_P from 7.6 to 6.6
476 km s^{-1} with a corresponding increase in v_P/v_S from 1.79 to 2.01. There is no evidence for
477 v_P/v_S >1.9 in either the Aleutians (Shillington et al., 2013) or LAA (Arnaiz-Rodrigues et al,
478 2016), ruling out variability in interconnected melt fraction as the principal cause of lateral v_P
479 gradients. Nonetheless, it is likely, given the active nature of these arcs, that some isolated
480 pockets of higher melt fraction exist, beyond the resolution of the seismic methods used.
481 Alternatively, it may be that the wetting properties of hydrous andesite and basaltic andesite
482 melts lead to less melt connectivity and consequently less extreme increase in v_P/v_S than
483 obtained by Chantel et al. (2016).
484
485 Normal faults orthogonal to the arc (e.g., Feuillet et al., 2002) could also lead to abrupt lateral
486 variations in crustal structure. However, the apparent decoupling of upper, mid and lower
487 crustal layer thicknesses mitigates against such an explanation. Variations in thickness of the
488 pre-subduction crust on the over-riding plate may also play a role, but, as noted above, this is
489 hard to evaluate from the seismic data alone. It seems more likely that normal faults, where
490 present, act to accommodate lateral thickness (and density) variations, for example through
491 isostatic readjustment, rather than create them. Evidence for relative vertical movements
492 along the LAA comes from observation of drowned coral reefs. For example, at Les Saintes,
493 Guadeloupe, Leclerc et al. (2014), estimate subsidence rates of 0.4 mm/yr over the past 125

kyr. Leclerc et al. (2015) derive a similar subsidence rate (0.3 mm/yr) for drowned reefs off the coast of Martinique. This subsidence is ascribed to arc-parallel extension (Feuillet et al., 2002), but could conceivably be driven instead by vertical block movement in response to lateral variation in crustal thickness and/or density. In ductile crust vertical motion driven by lateral density gradients has been proposed as a mechanism for generating crustal stratification (e.g. Glazner, 1994) and may ultimately lead to sinking of dense, lower crustal cumulates into the mantle, i.e. delamination (Jagoutz & Behn, 2013). However, the positive (albeit non-linear) correlation of v_P and density (Fig. 6b; Supplementary Table S2) does not support a convective process, unless it is enhanced by a significant fraction of partial melt serving to reduce the density of higher v_P cumulates. We argue above that such melt, if present, cannot be significant in volume and/or interconnected.

Our preferred interpretation of LAA crustal structure is along-arc variation in the mechanisms of melt generation and differentiation. These variations can arise from instabilities along the mantle-slab interface, such as those predicted by the numerical models of Gerya et al. (2006), or by generation of hot, buoyant regions within the mantle wedge, as demonstrated by Tamura et al. (2002) for northern Japan. Tamura et al. (2002) suggest that low velocity regions in the crust are linked to “hot fingers” in the underlying mantle. It is not clear whether the generation of “hot fingers” is due to lateral variations in wedge temperature or in the proportion of partial melt generated by the influx of slab-derived fluids, or a combination of both. In Gerya et al’s (2006) numerical models upwellings, or “cold plumes”, arising from the slab interface generate lateral variations in melt productivity and composition within the mantle wedge. The finger-like protuberances of high- and low-v_P crustal material observed in Figure 8 could correspond to the influence of cold plumes as they impinge on the over-riding plate or to the rise of hot fingers. Both features afford a

519 mechanism for arc-parallel, convective motion in the mantle wedge that could drive along-arc
520 variability in magma flux and chemistry. Along-arc flow of the asthenosphere has been
521 proposed as an explanation of trench-parallel seismic anisotropy beneath the Tonga-
522 Kermadec and the Marianas arcs (e.g., Menke et al., 2015; Smith et al., 2001). However, the
523 pattern of anisotropy in the upper-mantle wedge tends to be highly variable, suggesting
524 variations in the style of upper-mantle flow from one subduction zone to another.
525
526 Generation of buoyant anomalies in the mantle wedge may, in part, be controlled by the
527 amount of water liberated from the slab (e.g., by serpentine dehydration) that can change
528 mantle density both by metasomatism (e.g. formation of amphibole or phlogopite peridotite)
529 and partial melting. This explanation is consistent with the observations of Schlaphorst et al.
530 (2016), based on b-value variations in upper plate seismicity along LAA, and on variations in
531 the ratio of fluid mobile and immobile trace elements in magmas along the Aleutians (Manea
532 et al., 2014). Seismic anomalies related to heterogeneous upwelling in the mantle wedge
533 beneath the Izu-Bonin arc have been observed by Obana et al. (2010), who also implicate
534 them in lateral variations in both crustal structure and magma chemistry.
535
536 Lateral variations in the magma differentiation mechanisms along the arc also play a role. It
537 is now recognised that many crustal magmatic systems comprise vertically extensive
538 magmatic mushes (Cashman et al. 2017), wherein differentiation occurs not by simple crystal
539 settling from a dominantly liquid magma chamber, but by upwards, reactive flow of buoyant,
540 low-degree melts through a crystal-rich (mush) framework. The products of such reactions, in
541 terms of solid residues, are modulated by the composition (especially H_2O content) and flux
542 of the basaltic, mantle-derived magmas feeding the base of the crust and the internal
543 architecture of the mush itself (Solano et al. 2012). Variations in input magma chemistry and

544 flux could be driven by the heterogeneous upwelling phenomena described above. Different
545 magma compositions and intensities of upwelling along the arc would drive different types of
546 mush reservoirs and, consequently, solid residue lithologies. The igneous xenolith record for
547 LAA is consistent with a laterally variable, mushy system, variously infiltrated and modified
548 by melts (Tollan et al. 2012; Stamper et al. 2014; Cooper et al. 2016; Melekhova et al. 2017,
549 Camejo-Harry et al. 2018), as demonstrated by variations in modal mineralogy along the arc
550 (Fig. 5). Melt infiltration drives reactions that produce diverse eruptible melts and variously
551 amphibole-bearing and amphibole-free plutonic rocks with differing physical properties (Fig.
552 6). The migration of v_P contours up and down the crustal column would then reflect the
553 changing mineralogy of the solid residues as partial melts migrate and react upwards.
554
555 In general, solid residues (xenoliths) become more magnesian (higher v_P) with depth (Fig. 5)
556 consistent with polybaric differentiation of mantle-derived magmas (Melekhova et al. 2015).
557 It is unclear whether the 7.8 km s^{-1} contour in Fig. 9 marks the crustal-mantle boundary (i.e.
558 Moho *sensu strictu*), or the change from mafic to ultramafic cumulates. As noted above and
559 by Müntener & Ulmer (2006), mantle peridotite and ultramafic cumulates have strikingly
560 similar physical properties that are not readily resolved by the seismic methods employed
561 here. The difficulty of recognising the Moho in the LAA, and in arcs more generally, likely
562 reflects the preponderance of ultramafic cumulates at depth, as proposed for the fossil
563 Kohistan arc by Jagoutz & Behn (2013).
564

565 # 6. Conclusions

566 We have elucidated crustal structure along strike in the LAA using a novel approach that
567 integrates xenolith petrology and seismology. Our approach affords several advantages over a
568 purely seismological approach, especially in arc settings at stations with significant noise,

where the H–κ stacking method is prone to ambiguity. Combining several local networks, it has been possible to generate a detailed picture of crustal structure beneath the major islands of LAA. We show that arc crust is highly variable along-arc on relatively short wavelengths. One explanation for such variability in the delivery of water to the arc, plausibly via heterogeneous mantle upwellings that in turn affect the temperature and composition of the mantle-derived melts supplied to the base of the crust (e.g., Parman et al 2011) and the solid residues produced during differentiation (e.g., Melekhova et al., 2015). We tentatively note a spatial correlation between changes in crustal v_P and subducting transform faults (Fig. 2), that are likely water-rich and serpentinised, as previously suggested by Schlaphorst et al. (2016). In relatively low productivity arcs, such as LAA, crust appears to be composed predominantly of the solid residues of differentiation processes, with little interstitial trapped melt. This process is distinct from a classical model of crustal differentiation in which solids progressively separate from large volumes of melt in crustal magma chambers. Thus, the mush-dominated architecture that appears to dominate many crustal magmatic systems (Cashman et al., 2017) may also control the structure of the arc crust. Using magmatic xenoliths to reconstruct crustal velocity structure is clearly a fruitful avenue that is complimentary to seismic experiments and to the reconstruction of seismic velocities from exhumed arc sections.

Data Access Statement: All underlying data are provided in full within this paper, either in the main text or as accompanying supplementary material.

Acknowledgements

This work was supported by NERC grants NE/N001966/1, NE/K004883/1, NE/K014978/1 and NE/K010824/1 and ERC Advanced Grant CRITMAG (Blundy). We thank S. Sparks and

members of the NERC-funded VoiLA research consortium (NE/K010824/1) for useful discussions, C. Hawkesworth for insightful comments and suggestions for the manuscript, T. Nichols for providing some of the xenolith modes from St. Lucia, and Y. Tamura and O. Jagoutz for reviews of the manuscript.

References

Ammon, C., Randall, G., Zandt, G., 1990. On the Non-uniqueness of Receiver Function Inversion. Geophysical Journal International 95, 15303–15318. doi:10.1029/JB095iB10p15303.

Arculus, R.J., Wills, K.J., 1980. The petrology of plutonic blocks and inclusions from the Lesser Antilles island arc. Journal of Petrology 21, 743–799.

Arnaiz-Rodríguez, M.S., Schmitz, M., Audemard, F., 2016. La estructura cortical del arco de las Antillas Menores estimada a partir de la técnica de funciones receptoras. Revista mexicana de ciencias geológicas 33, 286–296.

Bezard, R., Davidson, J.P., Turner, S., Macpherson, C.G., Lindsay, J.M., Boyce, A.J., 2014. Assimilation of sediments embedded in the oceanic arc crust: myth or reality? Earth and Planetary Science Letters 395, 51-60. doi.org:10.1016/j.epsl.2014.03.038

Bezard, R., Turner, S., Davidson, J.P., Macpherson, C.G. and Lindsay, J.M., 2015. Seeing through the effects of crustal assimilation to assess the source composition beneath the southern Lesser Antilles Arc. Journal of petrology, 56, 815-844. doi: 10.1093/petrology/egv018

Bouvier, A. S., Metrich, N. & Deloule, E., 2008. Slab-derived fluids in the magma sources of St. Vincent (Lesser Antilles arc): volatile and light element imprints. Journal of Petrology 49,1427–1448. doi.org:10.1093/petrology/egn031

Boynton, C., Westbrook, G., Bott, M., Long, R., 1979. A seismic refraction investigation of crustal structure beneath the Lesser Antilles arc. Geophysical Journal of the Royal Astronomical Society 58, 371–393.

Camejo-Harry, M., Melekhova, E., Blundy, J., Attridge, W., Robertson, R. and Christopher, T., 2018. Magma evolution beneath Bequia, Lesser Antilles, deduced from petrology of lavas and plutonic xenoliths. Contributions to Mineralogy and Petrology, 173, 77, doi.org:10.1007/s00410-018-1504-z

Cashman, K.V., Sparks, R.S.J., Blundy, J.D., 2017. Vertically extensive and unstable magmatic systems: A unified view of igneous processes. Science 355, eaag3055. doi:10.1126/science.aag3055.

Chantel, J., Manthilake, G., Andrault, D., Novella, D., Yu, T., Wang, Y., 2016. Experimental evidence supports mantle partial melting in the asthenosphere. Science advances 2, e1600246. doi:10.1126/sciadv.1600246.

Christeson, G., Mann, P., Escalona, A., Aitken, T., 2008. Crustal structure of the Caribbean-northeastern South America arc-continent collision zone. Journal of Geophysical Research–Solid Earth 113. doi:10.1029/2007JB005373.

Cooper, G.F., Davidson, J.P., Blundy, J.D., 2016. Plutonic xenoliths from Martinique, Lesser Antilles: evidence for open system processes and reactive melt flow in island arc crust. Contributions to Mineralogy and Petrology 171, 87. doi:10.1007/s00410-016-1299-8.

644 Feuillet, N., Manighetti, I., Tapponnier, P., Jacques, E., 2002. Arc parallel extension and localization of volcanic
645 complexes in Guadeloupe, Lesser Antilles. Journal of Geophysical Research Solid Earth 107, B12.
646 doi: 10.1029/2001JB000308.
647
648 Gailler, L.S., Martelet, G., Thinon, I., Bouchot, V., Lebrun, J.F., Münch, P., 2013. Crustal structure of
649 Guadeloupe islands and the Lesser Antilles arc from a new gravity and magnetic synthesis. Bulletin de la
650 Société Géologique de France 184, 77–97. doi:10.2113/gssgfbull.184.1-2.77.
651
652 Gerya, T.V., Connolly, J.A., Yuen, D.A., Gorczyk, W., Capel, A.M., 2006. Seismic implications of mantle
653 wedge plumes. Physics of the Earth and Planetary Interiors 156, 59–74. doi:10.1016/j.pepi.2006.02.005.
654
655 Gianola, O., Schmidt, M.W., Jagoutz, O., Sambuu, O., 2017. Incipient boninitic arc crust built on denudated
656 mantle: the Khantaishir ophiolite (western Mongolia). Contributions to Mineralogy and Petrology 172, 92.
657 doi:10.1007/s00410-017-1415-4.
658
659 Glazner, A.F., 1994. Foundering of mafic plutons and density stratification of continental crust. Geology, 22,
660 435-438. doi.org:10.1130/0091-7613(1994)022<0435:FOMPAD>2.3.CO;2
661
662 Hacker, B.R., Abers, G.A., 2004. Subduction factory 3: An excel worksheet and macro for calculating the
663 densities, seismic wave speeds, and H2O contents of minerals and rocks at pressure and temperature.
664 Geochemistry, Geophysics, Geosystems 5. doi:10.1029/2003GC000614.
665
666 Hammond, J., Kendall, J.M., GW, S., Keir, D., Ebinger, C., Ayele, A., Belachew, M., 2011. The nature of the
667 crust beneath the Afar triple junction: Evidence from receiver functions. Geochemistry Geophysics Geosystems
668 12. doi:10.1029/2011GC003738.
669
670 Helffrich, G., 2006. Extended-time multitaper frequency domain cross-correlation receiver-function estimation.
671 Bulletin of the Seismological Society of America 96, 344–347. doi.org:10.1785/0120050098
672
673 Ishizuka, O., Hickey-Vargas, R., Arculus, R.J., Yogodzinski, G.M., Savov, I.P., Kusano, Y., McCarthy, A.,
674 Brandl, P.A. and Sudo, M., 2018. Age of Izu–Bonin–Mariana arc basement. Earth and Planetary Science
675 Letters, 481, pp.80-90. doi.org:10.1016/j.epsl.2017.10.023
676
677 Jagoutz, O., Behn, M.D., 2013. Foundering of lower island-arc crust as an explanation for the origin of the
678 continental Moho. Nature, 504, 131-134
679
680 Jicha, B.R., Jagoutz, O., 2015. Magma production rates for intraoceanic arcs. Elements 11, 105–111.
681 doi:10.2113/gselements.11.2.105.
682
683 Jull, M., Kelemen, P.B., 2001. On the conditions for lower crustal convective instability. Journal of Geophysical
684 Research: Solid Earth 106, 6423–6446. doi:10.1029/2000JB900357.
685
686 Kiddle, E., Edwards, B., Loughlin, S., Petterson, M., Sparks, R., Voight, B., 2010. Crustal structure beneath
687 Montserrat, Lesser Antilles, constrained by xenoliths, seismic velocity structure and petrology. Geophysical
688 Research Letters 37. doi:10.1029/2009GL042145.
689
690 Kodaira, S., Sato, T., Takahashi, N., Tamura, Y., Tatsumi, Y., Kaneda, Y., 2007. Seismological evidence for
691 variable growth of crust along the Izu intraoceanic arc. Journal of Geophysical Research–Solid Earth 112.
692 doi.org/10.1029/2006JB004593.
693
694 Kopp, H., Weinzierl, W., Becel, A., Charvis, P., Evain, M., Flueh, E., Gailler, A., Galve, A., Hirn, A.,
695 Kandilarov, A., Klaeschen, D., Laigle, M., Papenberg, C., Planert, L., Roux, E., Team, T., Team, T., 2011. Deep
696 structure of the central Lesser Antilles Island Arc: Relevance for the formation of continental crust. Earth and
697 Planetary Science Letters 304, 121–134. doi:10.1016/j.epsl.2011.01.024.
698
699 Laigle, M., Hirn, A., Sapin, M., Bécel, A., Charvis, P., Flueh, E., Diaz, J., Lebrun, J.F., Gesret, A., Raffaele, R.
700 and Galvé, A., 2013. Seismic structure and activity of the north-central Lesser Antilles subduction zone from an
701 integrated approach: Similarities with the Tohoku forearc. Tectonophysics, 603, pp.1-20.
702 doi:10.1016/j.tecto.2013.05.043
703

Leclerc, F., Feuillet, N., Cabioch, G., Deplus, C., Lebrun, J.F., BATHYSAINTES cruise scientific party, Bazin, S., Beauducel, F., Boudon, G., LeFriant, A., De Min, L., Melezan, D., 2014. The Holocene drowned reef of Les Saintes plateau as witness of a long-term tectonic subsidence along the Lesser Antilles volcanic arc in Guadeloupe. Marine Geology, 355, 115-135. doi.org:10.1016/j.margeo.2014.05.017

Leclerc, F., Feuillet, N., Perret, M., Cabioch, G., Bazin., S., Lebrun, J.-F., Saurel, J.M., 2015. The reef platform of Martinique: Interplay between eustasy, tectonic subsidence and volcanism since Late Pleistocene. Marine Geology, 369, 34-51. doi.org:10.1016/j.margeo.2015.08.001

Macdonald, R., Hawkesworth, C. J. & Heath, E., 2000. The Lesser Antilles volcanic chain: a study in arc magmatism. Earth-Science Reviews 49, 1–76. doi.org:10.1016/S0012-8252(99)00069-0.

Manea, V.C., Leeman, W.P., Gerya, T., Manea, M. and Zhu, G., 2014. Subduction of fracture zones controls mantle melting and geochemical signature above slabs. Nature communications 5, 5095.doi: 10.1038/ncomms6095

Melekhova, E., Blundy, J., Robertson, R., Humphreys, M.C., 2015. Experimental evidence for polybaric differentiation of primitive arc basalt beneath St. Vincent, Lesser Antilles. Journal of Petrology 56, 161–192. doi.org:10.1093/petrology/egu074

Melekhova, E., Blundy, J., Martin, R., Arculus, R., Pichavant, M., 2017. Petrological and experimental evidence for differentiation of water-rich magmas beneath St. Kitts, Lesser Antilles. Contributions to Mineralogy and Petrology 172, 98. doi.org:10.1007/s00410-017-1416-3

Menke, W., Y. Zha, S. C., Webb, D. K., Blackman., 2015. Seismic anisotropy indicates ridge-parallel asthenospheric flow beneath the Eastern Lau Spreading Center, J. Geophys. Res. Solid Earth., 120, pg. 976–992, doi:10.1002/2014JB011154

Müntener, O., Ulmer, P., 2006. Experimentally derived high-pressure cumulates from hydrous arc magmas and consequences for the seismic velocity structure of lower arc crust. Geophysical Research Letters 33. doi:10.1029/2006GL027629.

Nandedkar, R.H., Ulmer, P., Müntener, O., 2014. Fractional crystallization of primitive, hydrous arc magmas: an experimental study at 0.7 GPa. Contributions to Mineralogy and Petrology 167, 1015. doi:10.1007/ s00410-014-1015-5. doi: 10.1007/s00410-014-1015-5

Obana, K., Kamiya, S., Kodaira, S., Suetsugu, D., Takahashi, N., Takahashi, T., Tamura, Y., 2010. Along-arc variation in seismic velocity structure related to variable growth of arc crust in northern Izu-Bonin intraoceanic arc. Geochemistry, Geophysics, Geosystems 11. doi:10.1029/2010GC003146. q08012.

Parkinson, I. J., Arculus, R. J. & Eggins, S. M., 2003. Peridotite xenolith from Grenada, Lesser Antilles Island Arc. Contribution to Mineralogy and Petrology 146, 241–262

Rudnick, R.L., Fountain, D.M., 1995. Nature and composition of the continental crust: a lower crustal perspective. Reviews of geophysics 33, 267–309. doi:10.1029/95RG01302.

Schlaphorst, D., Kendall, J., Collier, J., Verdon, J., Blundy, J., Baptie, B., Latchman, J., Massin, F., Bouin, M., 2016. Water, oceanic fracture zones and the lubrication of subducting plate boundaries – insights from seismicity. Geophysical Journal International 204, 1405–1420. doi:10.1093/gji/ggv509.

Schlaphorst, D., Melekhova, E., Kendall, J-M., Blundy, J., Latchman, J.L., 2018. Probing layered arc crust in the Lesser Antilles using receiver functions. R. Soc. open sci. 5:180764. doi.org:10.1098/rsos.180764

Shillington, D.J., Van Avendonk, H.J., Holbrook, W.S., Kelemen, P.B., Hornbach, M.J., 2004. Composition and structure of the central Aleutian island arc from arc-parallel wide-angle seismic data. Geochemistry, Geophysics, Geosystems 5. doi:10.1029/2004GC000715.

Shillington, D.J., Van Avendonk, H.J.A., Behn, M.D., Kelemen, P.B., Jagoutz, O., 2013. Constraints on the composition of the Aleutian arc lower crust from VP/VS. Geophysical Research Letters, 40, 2579–84. doi.org:10.1002/grl.50375

Smith, G. P., Wiens, D.A. Fischer, M., Dorman, L., Webb., S., Hildebrand, J. (2001). A complex pattern of mantle flow in the Lau Backarc, Science, 292, 713–716. doi:10.1126/science.1058763

Smith, A.L., Roobol, M.J., Mattioli, G.S., Fryxell, J.E., Daly, G., Fernandez, L.A., 2013. The Volcanic Geology of the Mid-Arc Island of Dominica. Volume 496. Geological Society of America.

Solano, J., Jackson, M., Sparks, R., Blundy, J., Annen, C., 2012. Melt segregation in deep crustal hot zones: a mechanism for chemical differentiation, crustal assimilation and the formation of evolved magmas. Journal of Petrology 53, 1999–2026. doi:10.1093/petrology/egs041.

Stamper C.C., Blundy, J., Arculus, R.J., Melekhova, E., 2014. Petrology of plutonic xenoliths and volcanic rocks from Grenada, Lesser Antilles. Journal of Petrology 55, 1353-1387, doi:10.1093/petrology/egu027

Tamura, Y., Tatsumi, Y., Zhao, D., Kido, Y., Shukuno, H., 2002 Hot fingers in the mantle wedge: new insights into magma genesis in subduction zones. Earth and Planetary Science Letters,197, 105-116. doi.org:10.1016/S0012-821X(02)00465-X.

Tamura, Y., Sato T., Fujiwara, T., Kodaira, S., Nichols A., 2016. Advent of continents: A new hypothesis. Scientific Report 6, 33517. doi:10.1038/srep33517.

Thompson, D., Bastow, I., Helffrich, G., Kendall, J.M., Wookey, J., Snyder, D., Eaton, D., 2010. Precambrian crustal evolution: Seismic constraints from the Canadian Shield. Earth and Planetary Science Letters 297, 655–666. doi.org/10.1016/j.epsl.2010.07.021

Tollan, P., Bindeman, I., Blundy, J., 2012. Cumulate xenoliths from St. Vincent, Lesser Antilles island arc: a window into upper crustal differentiation of mantle-derived basalts. Contributions to Mineralogy and Petrology 163, 189–208. doi:10.1007/s00410-011-0665-9.

Toothill, J., Williams, C., Macdonald, R., Turner, S., Rogers, N., Hawkesworth, C., Jerram, D., Ottley, C., Tindle, A., 2006. A complex petrogenesis for an arc magmatic suite, St Kitts, Lesser Antilles. Journal of Petrology 48, 3–42. doi:10.1093/petrology/egl052.

Wadge, G., 1986. The dykes and structural setting of the volcanic front in the Lesser Antilles island arc. Bulletin of Volcanology 48, 349–372. doi:10.1007/BF01074466.

Wills, K. J. A., 1974. The geological history of Southern Dominica and plutonic nodules from the Lesser Antilles. Unpublished Ph.D. Thesis, University of Durham, England.

Ziberna, L., Green, E.C., Blundy, J.D., 2017. Multiple-reaction geobarometry for olivine-bearing igneous rocks. American Mineralogist 102, 2349–2366. doi:10.2138/am-2017-6154.

Figure Captions

Figure 1. Comparison of crustal structure of a selection of intra-oceanic arcs based on seismic refraction experiments (updated and modified from Boynton et al., 1979). The range in v_P (km/s) within individual crustal layers is shown by the double-ended arrows; asterisks denote an average value for multiple layers. Seismic discontinuities are shown by solid horizontal lines; the Moho is indicated by an additional dotted line. A question mark indicates

a poorly resolved Moho. Fine dashed lines represent changes in v_P without associated discontinuity. References for the arcs are provided by Boynton et al. (1979) with the following additions: Lesser Antilles – (a: S of Grenada, Christeson et al. 2008; b: S of Guadeloupe, Kopp et al. 2011); Japan – (a: Honshu, Iwasaki et al. 2001); (b: Hokkaido, Iwasaki et al. 2004); Sunda – (Kieckhefer et al. 1980); Aleutians – (Shillington et al. 2004); Izu – (Kodaira et al. 2007); Mariana – (Takahashi et al. 2007).

Figure 2. Map of the Lesser Antilles arc showing the seismic broadband stations used in this study (red triangles) and newly deployed stations (in yellow) by VoiLA (a NERC-funded multidisciplinary consortium project). The western, active branch of the arc is shown in black, the eastern, inactive branch in grey. There are 12 seismic stations on Montserrat in close proximity. Approximate extrapolation of fracture zones from the downgoing plate to the sub-arc is illustrated by dotted black lines: FT – Fifteen-Twenty; Ma – Marathon; Me – Mercurius; Ve – Vema; Do – Doldrums (Schlaphorst et al. 2016).

Figure 3. Bulk-rock MgO (a) and Al_2O_3 (b) variations in Lesser Antilles lavas plotted against SiO_2. (c) Plot of SiO_2 against of FeO^T/MgO ratio. Data with measured FeO and Fe_2O_3 are marked by circles with a black outline on (a) and (b). Pink solid line on (c) corresponds to an FeO/MgO ratio that would correspond to equilibrium with olivine Fo_{90}, using $Kd^{ol\text{-}liq}$=0.3. Magmas that lie on or below this line are potentially primary, i.e. in equilibrium with mantle olivine $Fo_{\geq 90}$. Potential primary magmas in LAA are predominantly basalts. Note absence of high-MgO basalts in northern islands and abundance of high-Al_2O_3 basalts and basaltic andesites. Data are from GEOROC.

Figure 4. Photomicrographs of representative xenolith textures and compositions in plane-polarised (ppl) and cross-polarised light (xpl). **(a)** Clinopyroxenite (sample GR5-1) with adcumulate texture (ppl) from Grenada showing large, unzoned clinopyroxene and hornblende with minor iddingsitised olivine. **(b)** Clinopyroxene-gabbro (CR6) from Carriacou (xpl) with porphyritic-phaneritic texture showing clinopyroxene grains with partial reaction to amphibole, and abundant oxides. **(c)** Hornblende-bearing troctolite (xpl) with adcumulate texture (VS8) from St Vincent. **(d)** Hornblende gabbronorite (xpl) with mesocumulate texture from St. Lucia (SL63). **(e)** Olivine-hornblende gabbro (ppl) with adcumulate texture from Dominica (DC102), showing considerable alteration of olivine to iddingsite. **(f)** Granodiorite (xpl) from Guadeloupe (GD40) showing equigranular texture. Mineral abbreviations: cpx (clinopyroxene), opx (orthopyroxene), pl (plagioclase), ox (Fe-Ti oxides), id (iddingsite), qz (quartz).

Figure 5. Modal proportion of minerals by mass in crustal xenoliths along LAA, ordered from North to South. Xenoliths for individual islands are listed from bottom to top in order of decreasing Fo content of olivine, followed by Mg# of clinopyroxene, followed by An content of plagioclase. Data from Wills, 1974; Tollan et al., 2012; Stamper et al 2014; Cooper et al., 2016; Melekhova et al 2017; Camejo-Harry et al., 2018; unpublished - Supplementary Table S1. Notice more mafic nature and almost complete absence of orthopyroxene in xenoliths from the southern segment compared to central and northern segments. Arrows and letters denote samples shown on Figure 4.

Figure 6. Seismic properties of LAA xenoliths calculated using the algorithm of Hacker & Abers (2016). All xenoliths are crustal igneous rocks, except for mantle xenoliths marked with a cross. Phase proportions were obtained by point counting (Fig. 5); P-T conditions of

equilibration were estimated by thermobarometry and/or phase petrology. **(a)** v_P/v_S ratio versus v_P. Note fields of plagioclase-rich (≥80% plagioclase) xenoliths with relatively low v_P and high v_P/v_S (dashed grey line) and amphibole-rich (≥80% amphibole + plagioclase ± quartz) xenoliths (dashed purple line). **(b)** v_P versus density (ρ). Hornblende and clinopyroxene-rich compositions form Grenada, St Vincent and one from Montserrat show significantly higher velocities and densities compared to other xenolith lithologies. The lowest density and velocity xenoliths are granodiorites from Guadeloupe. **(c)** Relative depths, estimated from thermobarometry and phase petrology, versus v_P. Different layers evaluated by RF inversion are shown: UC – upper-crustal layer (2), MC – mid-crustal layer (3), LU – low-crustal layer (4) and M – mantle layer (5).

Figure 7. Modeled 1-D profiles for density, v_P and v_S (top) and Receiver Functions (bottom) for Martinique (A) and Grenada (B). Lower panels show the stacked RFs (black) and the model RFs (red); grey lines show the pointwise 2σ-jackknife uncertainties. Modelling results for all other islands can be found in Supplementary Material.

Figure 8. Compilation of inversion results along LAA from south (Grenada) to north (Statia). Along-arc bathymetry in the top panel was constructed using latitude-longitude-elevation data from the global multi-resolution topography (GMRT) synthesis via GeoMapApp, and the multi-point "path profiler" tool in GlobalMapper20. The bottom panel shows the crustal v_P structure beneath each island based on a five-layer inversion (four crustal layers plus mantle) using RFs and petrological constraints as described in the text. v_P values (km/s) of each layer are shown for clarity. The Moho is denoted by a thick black line. Note heterogeneity of the uppermost layer (1) and the abrupt lateral variations in v_P and crustal layer thicknesses. Note that only two crustal layers could be resolved beneath Montserrat.

884

885

886 **Figure 9.** Comparison of v_P structure beneath three oceanic arcs: (a) Northern segment of
887 Izu-Bonin (Kodaira et al, 2007); (b) Aleutians (Shillington et al. 2004); and (c) Lesser
888 Antilles (this study). Contour intervals of 6.0, 6.8 and 7.8 km s^{-1} are chosen to aid
889 comparison. All figures drafted to the same vertical and horizontal scale. Lesser Antilles
890 structure (c) adapted from Fig 8 using the method in Supplementary Information with
891 velocities between islands estimated using a third-order polynomial interpolation. Volcanic
892 islands denoted with triangles, using the following abbreviations: (a) Os – Oh-shima; Nij –
893 Nii-jima; Myk – Miyake-jima; Mkr – Mikura-jima; Krs – Kurose; Hcj – Hachijo-jima; Shc –
894 South Hachijo; Ags – Aoga-shima; Myn – Myojin; Sms – South Sumisu; Ssc – South
895 Sumisu; Tsm – Torishima; (b) Seg – Seguam; Am – Amukta; Yun – Yunaska; Her – Herbert;
896 Chu – Chuginadak; (c) Ski – St. Kitts; Seus – St. Eustatius (Statia). Note low velocity mid-
897 crustal layer under Grenada and Grenadines, and high velocity region under Statia. Izu-Bonin
898 and Aleutians seismic data were obtained at much higher resolution than for LAA, yet the
899 overall lateral variations in v_P structure and crustal thickness are similar in all three arcs.

Figure 1

Click here to download Figure: Figure 1.pdf

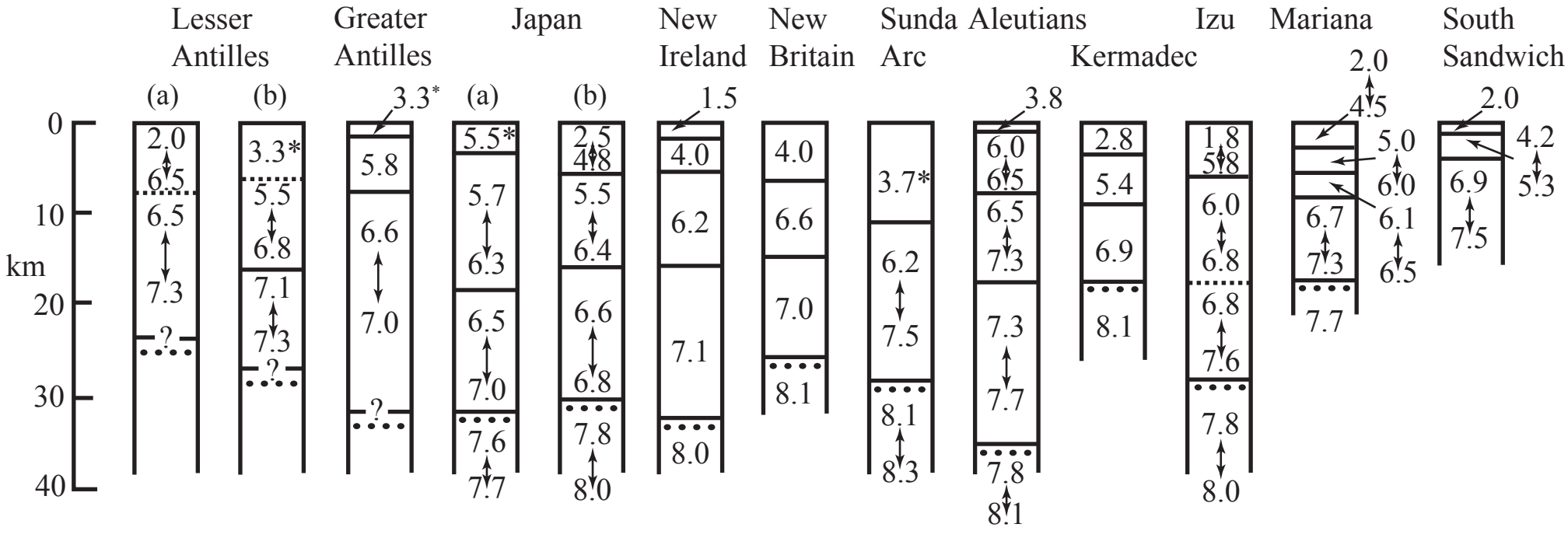

Figure 2

Click here to download Figure: Figure 2.pdf

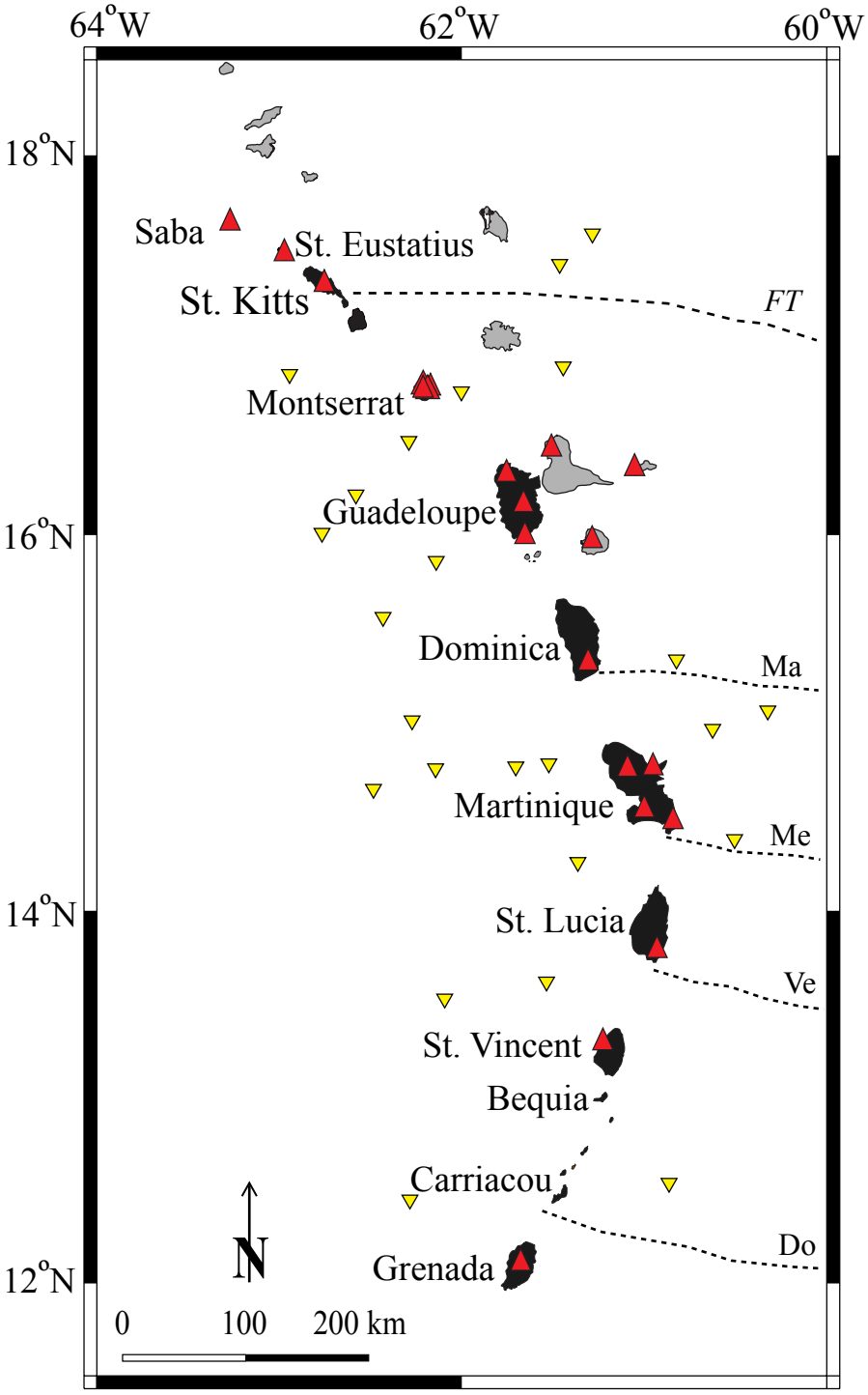

Figure 3

Click here to download Figure: Figure 3.pdf

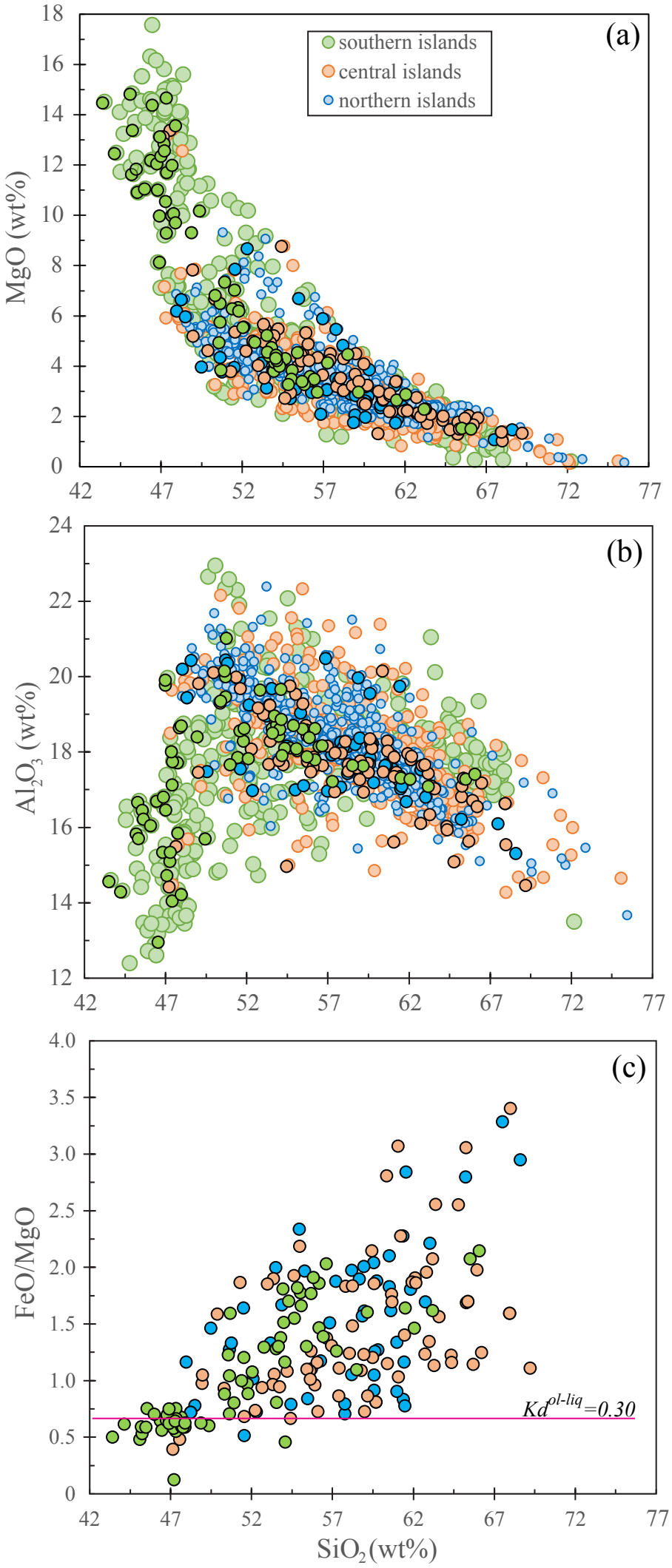

Figure 4

Click here to download Figure: Figure 4.pdf

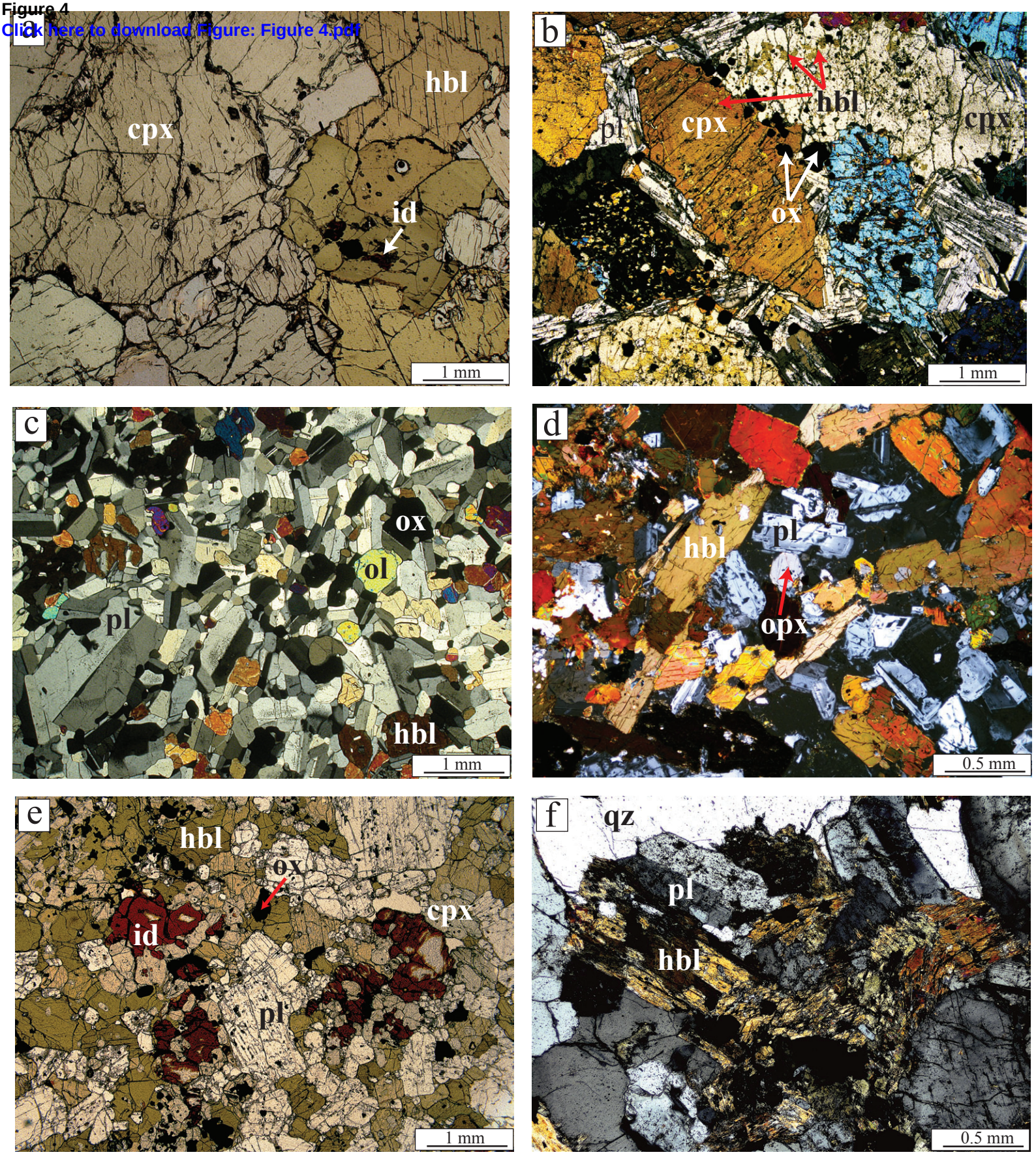

Figure 5

Click here to download Figure: Figure 5.pdf

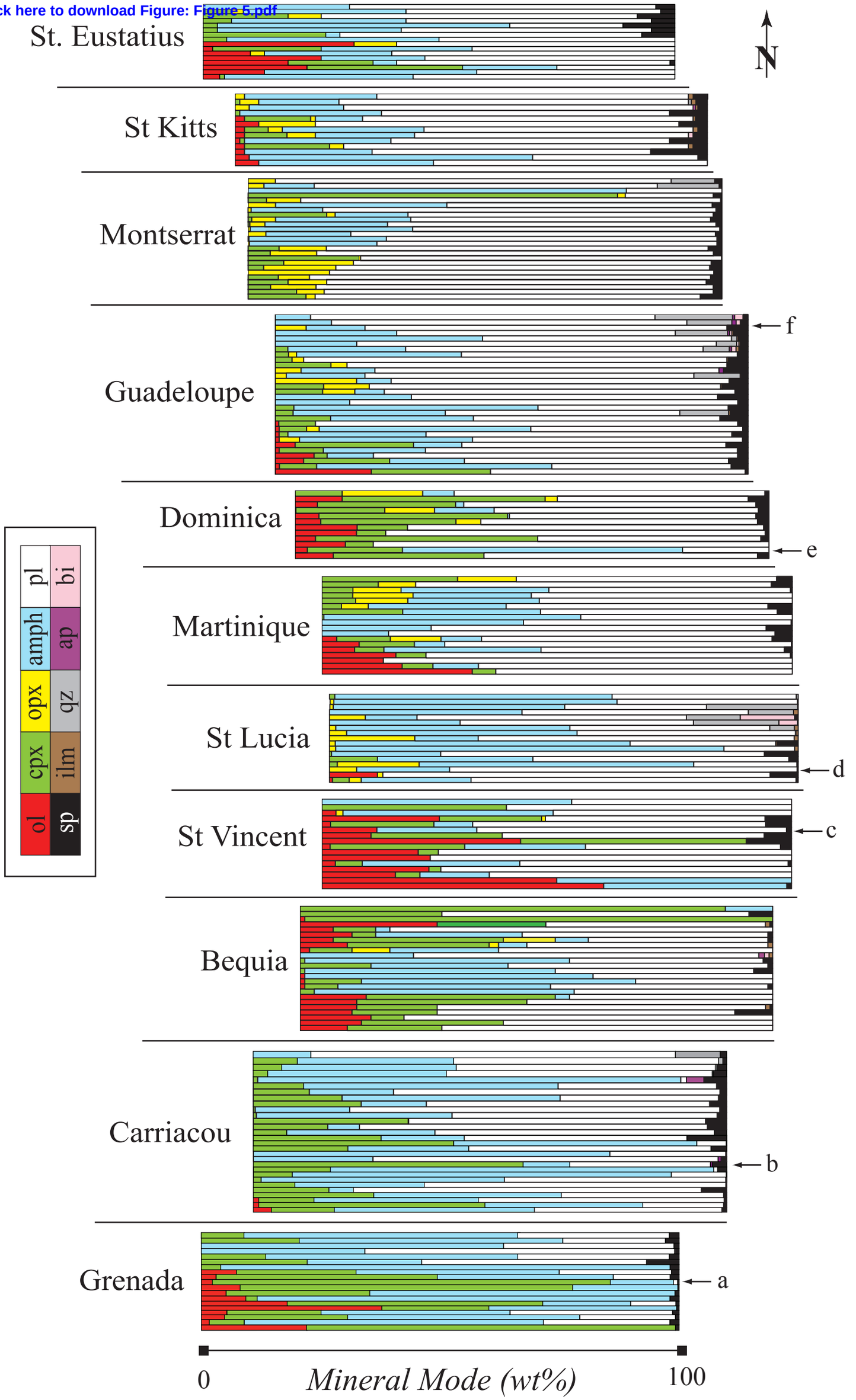

Figure 6

Click here to download Figure: Figure 6.pdf

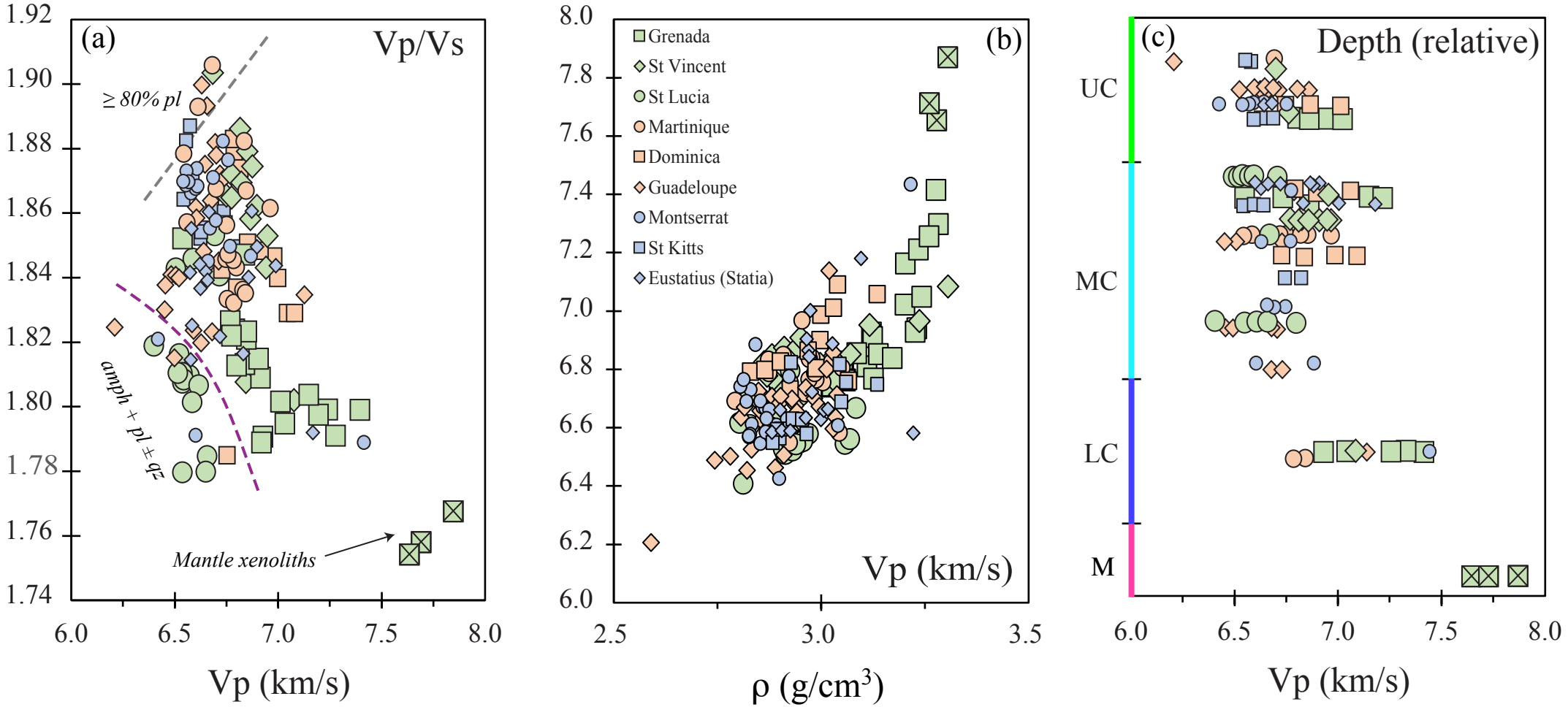

Figure 7

Click here to download Figure: Figure 7.pdf

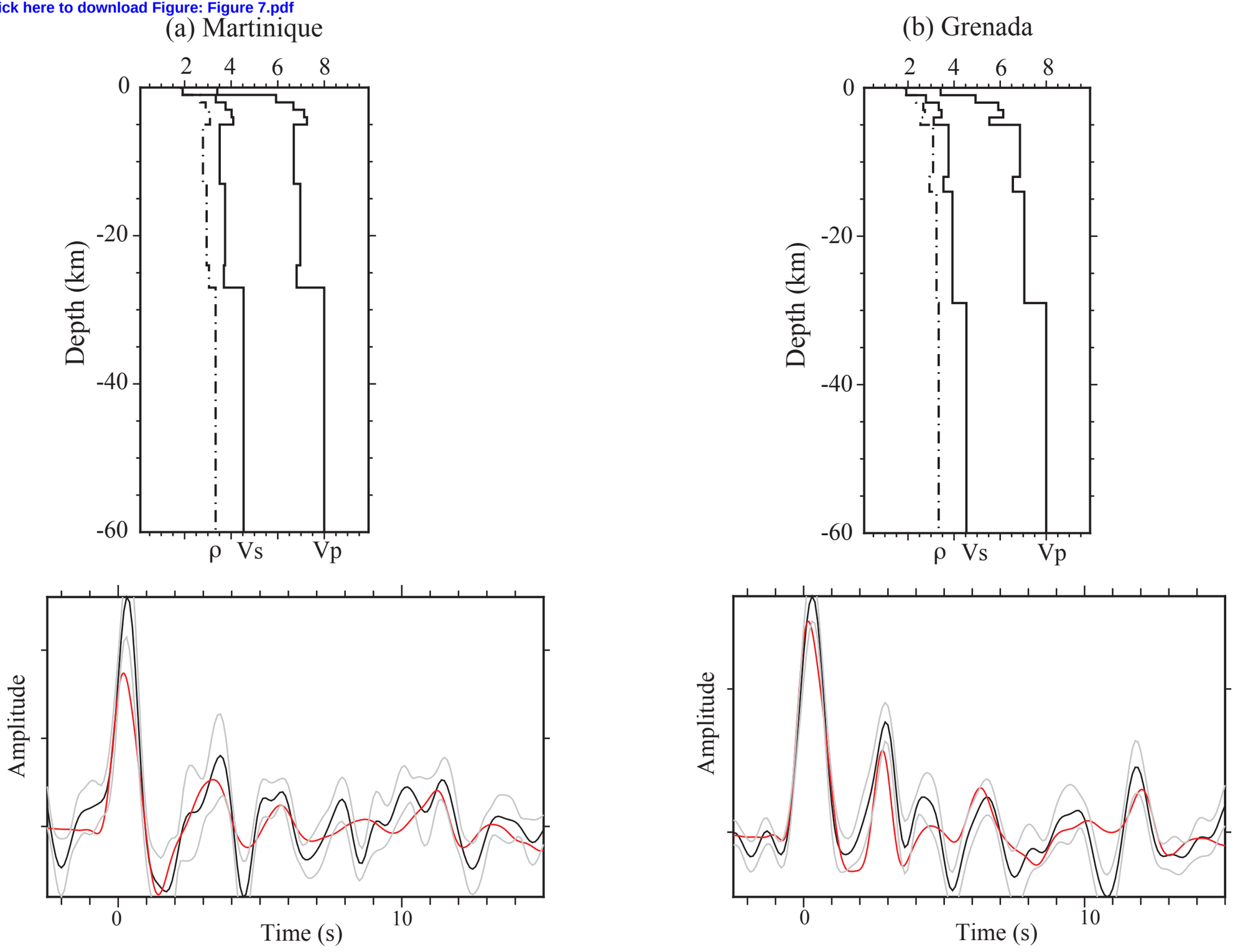

Figure 8
Click here to download Figure: Figure 8.pdf

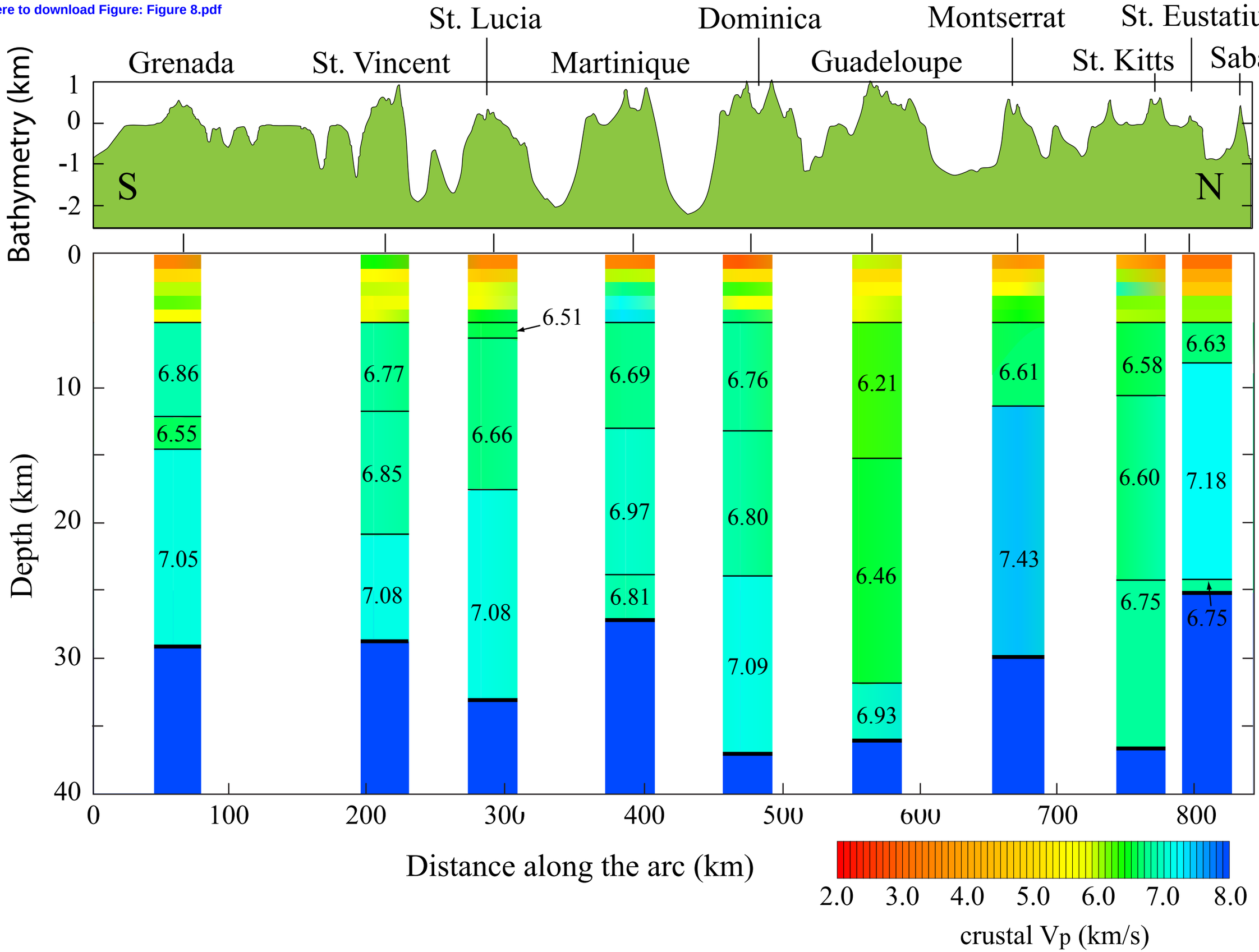

Figure 9

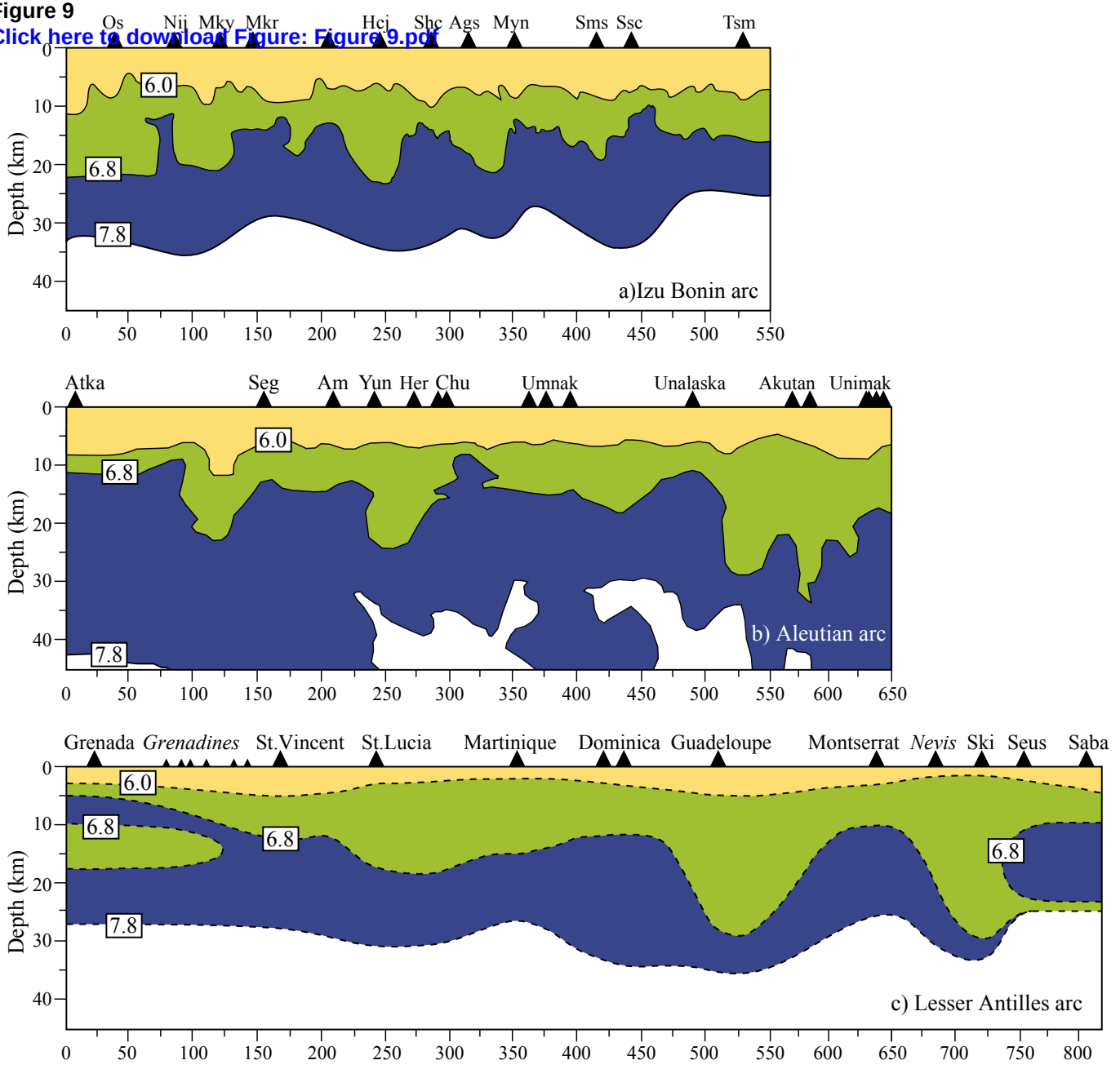

Figure 4 (high-resolution)

Click here to download Figure (high-resolution): Figure 4.tif

Table 1
Click here to download Table: Table 1.docx

Table 1. The modeled velocity profiles and MCD and Moho depth.

	Layer (2)	v_P (km/s)	r (g/cm^3)	z* (km)	Layer (3)	v_P (km/s)	r (g/cm^3)	z* (km)	Layer (4)	v_P (km/s)	r (g/cm^3)	z* (km)
Grenada	poikilitic-hornblende gabbro (GR4)	6.86	3.09	12	hornblende gabbro (GR42)	6.55	2.93	14	clinopyroxene hornblendite (GR17)	7.3	3.28	29
St. Vincent	hornblende troctolite (VS8)	6.77	2.88	12	plagioclase hornblendite (VS5)	6.85	3.07	21	olivine hornblende pyroxenite (VS20)	7.08	3.93	29
St. Lucia	hornblende leuco-norite (SL107)	6.51	2.91	6	hornblende norite (SL72)	6.66	2.89	17	olivine-hornblende pyroxenite (VS20)	7.08	3.93	33
Martinique	troctolite (MQ55)	6.69	2.79	13	olivine gabbro (MQ13)	6.97	2.95	24	hornblende gabbronorite (MQ12)	6.81	3.05	25
Dominica	olivine hornblende gabbro (D214)	6.76	3.07	13	olivine hornblende gabbronorite (D410)	6.80	2.99	23	olivine gabbro (D250c)	7.09	3.04	25
Guadeloupe	granodiorite (GD43)	6.21	2.59	15	diorite (GD39)	6.46	2.89	32	hornblendite (GR25)	6.93	3.23	36
Montserrat	–	-	-	-	plagioclase hornblendite (FB220)	6.61	3.04	11	plagioclase pyroxenite (300a)	7.43	3.22	30
St. Kitts	olivine norite (KS11)	2.96	6.58	10	olivine hornblende gabbro (KS22)	2.9	6.6	19	olivine hornblende gabbro (KS15)	6.75	3.14	37
St. Eustatius	hornblende gabbronorite (EU22)	6.63	2.96	8	olivine hornblende gabbro (EU77)	7.18	3.10	24	olivine hornblende gabbro (KS15)	6.75	3.14	25

z* - depth to the bottom of the layer

Supplementary Table S1

Click here to download Supplementary material for online publication only: Supp.Table S1.xlsx

Supplementary Table S2

Click here to download Supplementary material for online publication only: Supp.Table S2.xlsx

Supplementary RF modelling

Click here to download Supplementary material for online publication only: Supplementary Material_RFmodelling.pdf